Title

Focal organizing pneumonia in patients: differentiation from solitary bronchioloalveolar carcinoma using dual-energy spectral computed tomography.

Journal

American Journal of Translational Research, 12(7)

ISSN

1943-8141

Authors

Zhang, Guojin
Cao, Yuntai
Zhang, Jing
et al.

Publication Date

2020

Am J Transl Res 2020;12(7):3974-3983
www.ajtr.org /ISSN:1943-8141/AJTR0109840

Original Article

Focal organizing pneumonia in patients: differentiation from solitary bronchioloalveolar carcinoma using dual-energy spectral computed tomography

Guojin Zhang[1,2], Yuntai Cao[1,2], Jing Zhang[1,2], Zhiyong Zhao[1,2], Wenjuan Zhang[1,2], Lele Huang[1,2], Zhuoli Zhang[3], Junlin Zhou[2,4]

[1]Second Clinical School, Lanzhou University, Lanzhou, China; [2]Key Laboratory of Medical Imaging of Gansu Province, Lanzhou, China; [3]Department of Radiology, Northwestern University, Chicago, USA; [4]Department of Radiology, Lanzhou University Second Hospital, Lanzhou, China

Received February 25, 2020; Accepted June 19, 2020; Epub July 15, 2020; Published July 30, 2020

Abstract: Objective: To explore the utility of dual-energy spectral computed tomography (CT) in the differential diagnosis of focal organizing pneumonia (FOP) and solitary bronchioloalveolar carcinoma (S-BAC). Materials and methods: The institutional review board approved this study and waived the requirement for informed consent. It is a retrospective study. A total of 105 patients (62 with FOP and 43 with S-BAC) enrolled and all patients have contrast enhanced spectral CT including the arterial phase (AP) and venous phase (VP). During AP and VP, $CT_{40\ keV}$, $CT_{70\ keV}$, and $CT_{100\ keV}$ values, iodine concentration (IC), water concentration (WC), and effective atomic number (Zeff) were measured on monochromatic and iodine-based material decomposition images, and the slope of the spectral curve (λ_{Hu}) was calculated. The two-sample t-test was used to compare quantitative parameters, and receiver operating characteristic (ROC) curves were generated to calculate diagnostic efficacies. Results: For AP, $CT_{40\ keV}$ and $CT_{70\ keV}$ values, IC, WC, Zeff, $\lambda_{70\ keV}$, and $\lambda_{100\ keV}$ measurements, there were significantly higher in patients with S-BAC than in those with FOP ($P < 0.05$). However, these quantitative parameters of VP were significantly lower in patients with S-BAC than in those with FOP ($P < 0.05$). ROC curve analysis revealed that the combination of all quantitative parameters in AP and VP provided the best diagnostic performance in distinguishing S-BAC from FOP (area under the ROC curve, 93.1%; sensitivity, 95.3%; specificity, 77.4%). Conclusions: Dual-energy spectral CT has the potential to identify S-BAC and FOP.

Keywords: Bronchioloalveolar carcinoma, organized pneumonia, diagnosis, dual-energy CT

Introduction

Focal organizing pneumonia (FOP) is defined as failure to completely absorb pneumonia or delay regressive pneumonia [1]. Pneumonia usually subsides within 4 weeks after anti-infective treatment; however, approximately 5%-10% of patients are not completely cured [2-5]. Histologically, FOP is characterized by alveolar duct and endobronchial proliferating fibroblasts and myofibroblasts forming polypoid granulation tissue in the lumen, or chronic inflammatory changes in the bronchial mucosa and obstructive lesions in tissue bronchioles [1, 3-7].

FOP mainly presents as solitary, localized, peripheral lung nodules, or masses on chest imaging [8-12]. It is often difficult to distinguish between FOP and solitary bronchioloalveolar carcinoma (S-BAC), and undergo over-treatment such as needle biopsy or surgical resection [1, 3-6, 13]; therefore it is necessary to distinguish FOP from S-BAC. However, there are a few of overlapping signs between FOP and S-BAC on chest CT scan, which makes it hard to identify the two common lesions in lungs using conventional multidetector CT (MDCT) technology [14, 15].

Dual-energy spectral CT cannot only determine the density of the base material and its distribution, but also provide single-energy images at different keV levels and calculate the effective atomic number of the lesion or tissue according to the spectral curve obtained. Compared with conventional MDCT, dual-energy spectral CT is

Table 1. Demographic and clinical features of patients with S-BAC and FOP

Variable	S-BAC (n = 62)	FOP (n = 43)	*P*
Age (years)			0.14
Mean ± SD	59.13 ± 8.52	56.40 ± 10.28	
Median/Range	61 (36-78)	59 (31-74)	
Sex (%)			0.20
Male	33 (53.23%)	25 (58.14%)	
Female	29 (46.77%)	18 (41.86%)	
Smoking history* (%)			0.31
Yes	27 (43.55)	14 (32.56)	
No	35 (56.45)	29 (67.44)	
Symptoms (%)			0.95
Asymptomatic	13 (20.97)	9 (20.93)	
Cough	21 (33.87)	15 (34.88)	
Sputum	16 (25.80)	10 (23.26)	
Chest pain	8 (12.90)	3 (6.98)	
Hemoptysis	9 (14.51)	4 (9.30)	
Fever	7 (11.29)	3 (6.98)	
Dyspnea	6 (9.68)	2 (4.65)	

FOP: Focal organizing pneumonia, S-BAC: Solitary bronchioloalveolar carcinoma, SD: Standard deviation. *Smoking history is defined as follows: Yes, former and current smokers; No, never smoked.

a new imaging mode enabling multi-parameter and quantitative analysis, thus yielding more useful information [16, 17]. It has demonstrated clear advantages in differentiating benign and malignant lung lesions [18-20].

This study aimed to investigate the potential of dual-energy spectral CT to identify S-BAC and FOP.

Materials and methods

Patients

The study was approved by the Institutional Review Board and the Ethics Committee of the Lanzhou University Second Hospital (Lanzhou, China), and written informed consent was obtained from all patients. This study retrospectively analyzed data from 43 patients (25 males, 18 females; mean [± SD] age, 56.40 ± 10.28 years; median age, 59 years [range, 31-74 years]) who were diagnosed with FOP between January 2013 and August 2019. All patients exhibited local lung parenchyma abnormalities on chest CT scan, which was difficult to distinguish from S-BAC at this stage. In addition, 62 patients (33 males, 29 females; mean age, 59.13 ± 8.52 years; median age, 61 years [range, 36-78 years]) diagnosed with S-BAC were treated in the same period. The demographic and clinical characteristics of patients with S-BAC and FOP are summarized in **Table 1**.

Inclusion/exclusion criteria

Patients who fulfilled eligibility criteria were entered into this study: availability of preoperative thin-slice CT data on the picture archiving and communication system; lesion(s) first discovered and no treatment before admission; lesion(s) presenting as solitary nodules or masses on chest CT images; underwent surgical resection or biopsy, and were confirmed as FOP or S-BAC on pathology; no other malignant tumors; underwent dual-phase enhanced thoracic scanning under the mode of gemstone spectral imaging (GSI); and complete clinical data including sex, age, symptoms, and smoking history (divided into smokers [previous and current] and non-smokers [never smokers]).

Individuals with poor-quality imaging data, the presence of respiratory artifacts and other conditions affecting observation, and those with an interval between CT examination and subsequent surgery > 7 days, were excluded.

CT protocol

All patients underwent imaging using a Discovery CT750 HD (GE Healthcare, Waukesha, WI, USA) scanner. The following scanning parameters were used: tube voltage, 80 kVp and 140 kVp instantaneous switching; tube current, 375 mA; bulb rotation time, 0.7 s; pitch, 0.984:1; scanning field of view, 500 mm; collimator, 400 mm; and axial layer thickness and layer spacing, 5 mm. The scan range was from the thoracic entrance to the diaphragm. A total of 80-100 ml (1.2 mL/kg of body weight) of non-ionic iodine contrast agent (Ultravist 300, Bayer Pharma, Berlin, Germany) was injected through the anterior elbow vein using a high-pressure syringe (XD8000, Ulrich, Germany) at a rate of 3.5~4 ml/s. The arterial phase (AP) and venous phase (VP) GSI mode were scanned using the auto-tracking method 30 s and 60 s after contrast injection. The CT images in AP and VP were reconstructed, and an adaptive

iterative reconstruction algorithm was used to suppress the noise of the decomposed image; the reconstructed layer thickness and layer spacing were both 1.25 mm.

Image analysis

Two radiologists with 5 and 10 years' experience and blinded to patient clinical information and pathological results independently measured quantitative parameters using a workstation (ADW4.6, GE Healthcare), and reached consensus through discussion in cases of divergence. A circular or elliptical region of interest was placed in the area where the lesion was uniformly enhanced, avoiding as much as possible, visible areas of blood vessels, calcification, cavitation, necrosis, cystic changes and atelectasis that could affect outcome. When the lesion density was uniform, the area of the region of interest should be > 1/2 the maximum cross-sectional area of the lesion. When the density of the lesion is uneven, the area with the most components in the layer was selected for measurement. To ensure the consistency in the results, measurements were performed on three consecutive images, and the mean value was calculated. For all measurements, the size, shape and location of the region of interest were consistent in two stages by applying the copy and paste function. The GSI software automatically generated the CT value, iodine concentration (IC), water concentration (WC) and effective atomic number (Zeff) of the lesion at the individual energies of 40 keV-100 keV (10 keV intervals) and calculated the slope of the spectral curve. According to the equation: $\lambda_{70\ keV} = (CT_{40\ keV} - CT_{70\ keV})/(70-40)$; $\lambda_{100\ keV} = (CT_{40\ keV} - CT_{100\ keV})/(100-40)$, the CT values corresponding to the two energy levels (40 keV and 70 keV, 40 keV and 100 keV, respectively) are calculated by dividing the energy difference (30 keV, 60 keV, respectively).

Statistical analysis

Statistical analysis was performed using SPSS version 22.0 (IBM Corporation, Armonk, NY, USA). Quantitative data are expressed as mean ± standard deviation, and enumerative data are expressed as percentage. Quantitative parameters between S-BAC and FOP were statistically compared using the two-sample *t*-test; differences with $P < 0.05$ were considered to be statistically significant. For values that were statistically different, receiver operating characteristic (ROC) curves were generated to evaluate diagnostic efficiency, and the cut-off value, sensitivity, and specificity in the maximal Youden's index (YI) were calculated. Sensitivity is defined as the true positive rate, which reflects the ability to correctly diagnose a patient's disease. Specificity is defined as the true negative rate, which reflects the ability to correctly identify disease-free patients.

Results

Clinical features of patients

The clinical features of the patients are summarized in **Table 1**. There was no significant difference between the S-BAC and FOP groups in terms of age, sex, smoking history, or symptoms ($P > 0.05$).

Analysis of quantitative parameters

Two representative sets of images derived from a single spectral CT acquisition (section thickness, 1.25 mm) in a patient with FOP and one with S-BAC are presented in **Figures 1** and **2**, respectively. The quantitative parameters of spectral CT in S-BAC patients and FOP patients are compared in **Table 2** and **Figure 3**. There were significant differences in $CT_{40\ keV}$ (166.12 ± 11.93 Hounsfield units [HU] versus [vs] 157.80 ± 12.45 HU; $P < 0.01$), $CT_{70\ keV}$ (66.69 ± 9.28 HU vs 63.02 ± 8.55 HU; $P = 0.04$), $\lambda_{70\ keV}$ (3.31 ± 0.35 vs 3.16 ± 0.34; $P = 0.03$), $\lambda_{100\ keV}$ (2.04 ± 0.22 vs 1.92 ± 0.22; $P = 0.01$), IC (17.35 ± 1.68 100 μg/cm^3 vs 16.36 ± 1.61 100 μg/cm^3; $P = 0.03$) and Zeff (8.62 ± 0.11 vs 8.56 ± 0.09; $P = 0.01$) between the patients with S-BAC and the patients with FOP during the AP, and the former was higher than the latter (**Table 2**; **Figure 3**). Patients with S-BAC demonstrated a significantly lower $CT_{40\ keV}$ (136.05 ± 6.32 HU vs 144.67 ± 18.25 HU; $P < 0.01$), $CT_{70\ keV}$ (58.58 ± 4.83 HU vs 61.50 ± 8.33 HU; $P = 0.04$), $\lambda_{70\ keV}$ (2.58 ± 0.24 vs 2.77 ± 0.50; $P = 0.02$), $\lambda_{100\ keV}$ (1.59 ± 0.15 vs 1.70 ± 0.33; $p = 0.03$), IC (13.38 ± 1.13 100 μg/cm^3 vs 14.16 ± 1.50 100 μg/cm^3; $P < 0.01$) and Zeff (8.41 ± 0.08 vs 8.46 ± 0.16; $P = 0.04$) than did patients with FOP during the VP (**Table 2**; **Figure 3**). The $CT_{100\ keV}$ values and WC between patients with S-BAC and those with FOP during the AP and VP were indeterminate (**Table 2**).

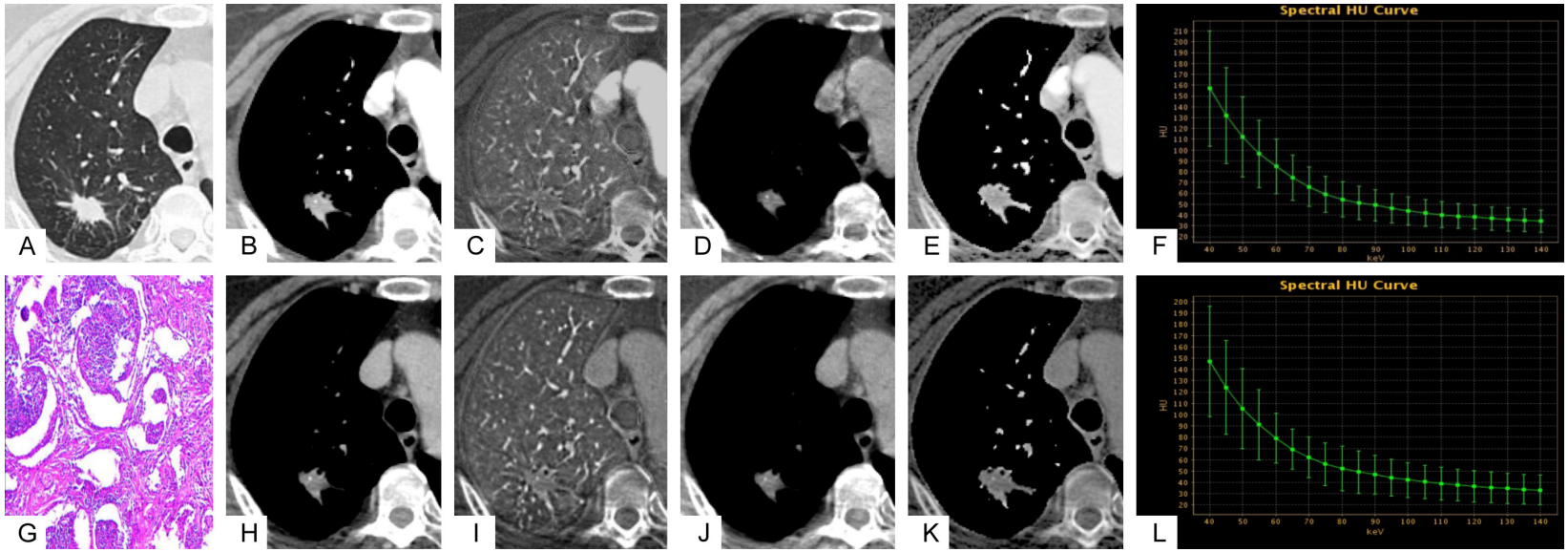

Figure 1. Spectral computed tomography (CT) images and pathological section of a 64-year-old woman with focal organizing pneumonia (FOP). Lung window (A), monochromatic CT image acquired at 70 keV energy level (B, H), iodine-based material decomposition image (C, I), water-based material decomposition image (D, J), effective atomic number (Zeff) (E, K) and spectral curve (F, L) in the arterial phase (AP) (B-F) and venous phase (VP) (H-L); (G) hematoxylin and eosin staining (original magnification × 200). $CT_{70\ keV}$ value in AP = 68.93 HU; $CT_{70\ keV}$ value in VP = 61.38 Hounsfield units (HU); iodine concentration (IC) in AP = 16.23 100 μg/cm^3; IC in VP = 15.06 100 μg/cm^3; water concentration (WC) in AP = 991.48 mg/cm^3; WC in VP = 993.81 mg/cm^3; Zeff in AP = 8.78; Zeff in VP = 8.70; slope of the spectral curve ($\lambda_{70\ keV}$) in AP = 2.99 HU; $\lambda_{70\ keV}$ in VP = 2.91 HU.

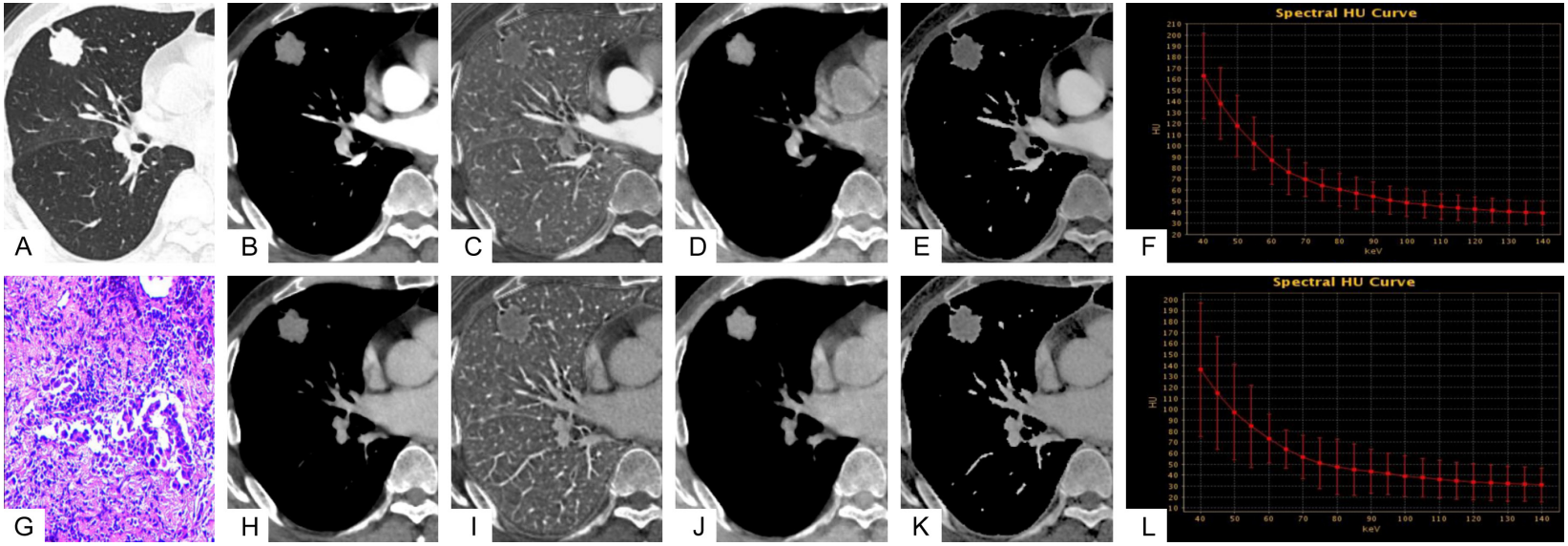

Figure 2. Spectral computed tomography (CT) images and the pathological section of a 66-year-old man with solitary bronchioloalveolar carcinoma (S-BAC). Lung window (A), monochromatic CT image obtained at 70 keV energy level (B, H), iodine-based material decomposition image (C, I), water-based material decomposition image (D, J), effective atomic number (Zeff) (E, K) and spectral curve (F, L) in the arterial phase (AP) (B-F) and venous phase (VP) (H-L); (G) hematoxylin and eosin staining (original magnification × 200). $CT_{70\ keV}$ value in AP = 70.29 Hounsfield units (HU); $CT_{70\ keV}$ value in VP = 57.42 HU; iodine concentration (IC) in AP = 16.07 100 μg/cm^3; IC in VP = 12.35 100 μg/cm^3; water concentration (WC) in AP = 1036.43 mg/cm^3; WC in VP = 1024.54 mg/cm^3; Zeff in AP = 8.49; Zeff in VP = 8.22; slope of the spectral curve ($\lambda_{70\ keV}$) in AP = 3.06 HU; $\lambda_{70\ keV}$ in VP = 2.66 HU.

Table 2. Comparison of parameter between S-BAC and FOP in AP and VP

Parameter	S-BAC (n = 62)	FOP (n = 43)	*t*	*P*
AP				
$CT_{40\ keV}$ (HU)	166.12 ± 11.93	157.80 ± 12.45	3.45	< 0.01
$CT_{70\ keV}$ (HU)	66.69 ± 9.28	63.02 ± 8.55	2.06	0.04
$CT_{100\ keV}$ (HU)	43.81 ± 10.02	42.32 ± 8.96	0.78	0.44
$\lambda_{70\ keV}$	3.31 ± 0.35	3.16 ± 0.34	2.25	0.03
$\lambda_{100\ keV}$	2.04 ± 0.22	1.92 ± 0.22	2.61	0.01
IC (100 μg/cm^3)	17.35 ± 1.68	16.36 ± 1.61	3.04	< 0.01
Zeff	8.62 ± 0.11	8.56 ± 0.09	2.53	0.01
WC (mg/cm^3)	1024.26 ± 11.23	1023.88 ± 10.03	0.18	0.86
VP				
$CT_{40\ keV}$ (HU)	136.05 ± 6.32	144.67 ± 18.25	-2.97	< 0.01
$CT_{70\ keV}$ (HU)	58.58 ± 4.83	61.50 ± 8.33	-2.07	0.04
$CT_{100\ keV}$ (HU)	40.48 ± 5.63	42.80 ± 8.53	-1.57	0.12
$\lambda_{70\ keV}$	2.58 ± 0.24	2.77 ± 0.50	-2.33	0.02
$\lambda_{100\ keV}$	1.59 ± 0.15	1.70 ± 0.33	-1.93	0.03
IC (100 μg/cm^3)	13.38 ± 1.13	14.16 ± 1.50	-2.88	< 0.01
Zeff	8.41 ± 0.08	8.46 ± 0.16	-2.10	0.04
WC (mg/cm^3)	1025.22 ± 6.73	1026.55 ± 10.26	-0.57	0.46

AP: Arterial phase, FOP: Focal organizing pneumonia, HU: Hounsfield, IC: Iodine concentration, S-BAC: Solitary bronchioloalveolar carcinoma, VP: Venous phase, WC: Water concentration, Zeff: Effective atomic number.

Diagnostic performance of quantitative parameters

The areas under the reader-specific ROC curves for all parameters (**Figure 4C**) for differentiating between S-BAC and FOP-especially those for the CT_{AP+VP} (0.864), the λ_{AP+VP} (0.866) and combination of all parameters (0.931) during the AP combine the VP-were > 0.85 (**Table 3**). However, the areas under the curves for only the CT_{AP}+λ_{AP}+IC+Zeff (0.787) during the AP was greater than 0.75 for differentiating between S-BAC and FOP (**Figure 4A**). And during the VP, only the CT_{VP} (0.802) and CT_{VP}+λ_{VP}+IC+Zeff (0.839) were > 0.80 (**Figure 4B**).

Using ROC curve analysis, the parameter threshold values required to optimize both the sensitivity and the specificity for differentiating between S-BAC and FOP were determined (**Table 3**). For example, during AP, when the Zeff threshold was 8.62, the sensitivity and specificity for distinguishing S-BAC from FOP were 53.2% and 88.4%, respectively. However, during the VP, when the Zeff threshold was 8.505, the sensitivity and specificity were 39.5% and 96.8%, respectively.

For the selected combination of optimal thresholds, the optimal sensitivity and specificity for distinguishing between S-BAC and FOP were the combination of CT_{AP+VP}+λ_{AP+VP}+IC_{AP+VP}+$Zeff_{AP+VP}$ during AP combined with VP and CT_{VP}+λ_{VP}+IC+Zeff during the VP (0.283 and 0.643, respectively) of 95.3% and 96.8%, respectively.

Discussion

FOP is often initially misdiagnosed as S-BAC and overtreated due to atypical signs and symptoms, as well as overlapping imaging features [8, 21, 22]. Therefore, it is important to accurately distinguish S-BAC from FOP before surgery. Hou et al. [19] reported that spectral CT imaging using quantitative parameters may be a promising new method to distinguish lung cancer from inflammatory masses. However, it is hard to identify S-BAC and FOP using conventional CT imaging. In our study, our results showed that dual-energy spectral CT has the potential to identify S-BAC and FOP.

Our results showed that $CT_{40\ kev}$ and $CT_{70\ kev}$ values, $\lambda_{70\ kev}$, $\lambda_{100\ keV}$, IC and Zeff for S-BAC patients were significantly higher than those for FOP patients in AP, while the results were the opposite in VP. According to pathological analysis, the above five indicators reflect the blood supply of the pulmonary mass. Zeff reflects the effective atomic number of inorganic materials in the region of interest. S-BAC is a subtype of lung adenocarcinoma that usually develops erratic angiogenesis and establishment of a vascular network [23-25]. FOP is caused by a long-term unabsorbed or delayed absorption of acute inflammation leading to significant proliferation of fibroblasts and myofibroblasts, which may result in a relative deficiency in microvascular density. This explains why the blood supply of patients with S-BAC in AP is more abundant than that of patients with FOP, and CT value (in HU), IC, and λ_{HU} are higher than that of the latter. In VP, because the blood reflux of patients with S-BAC is faster than that of

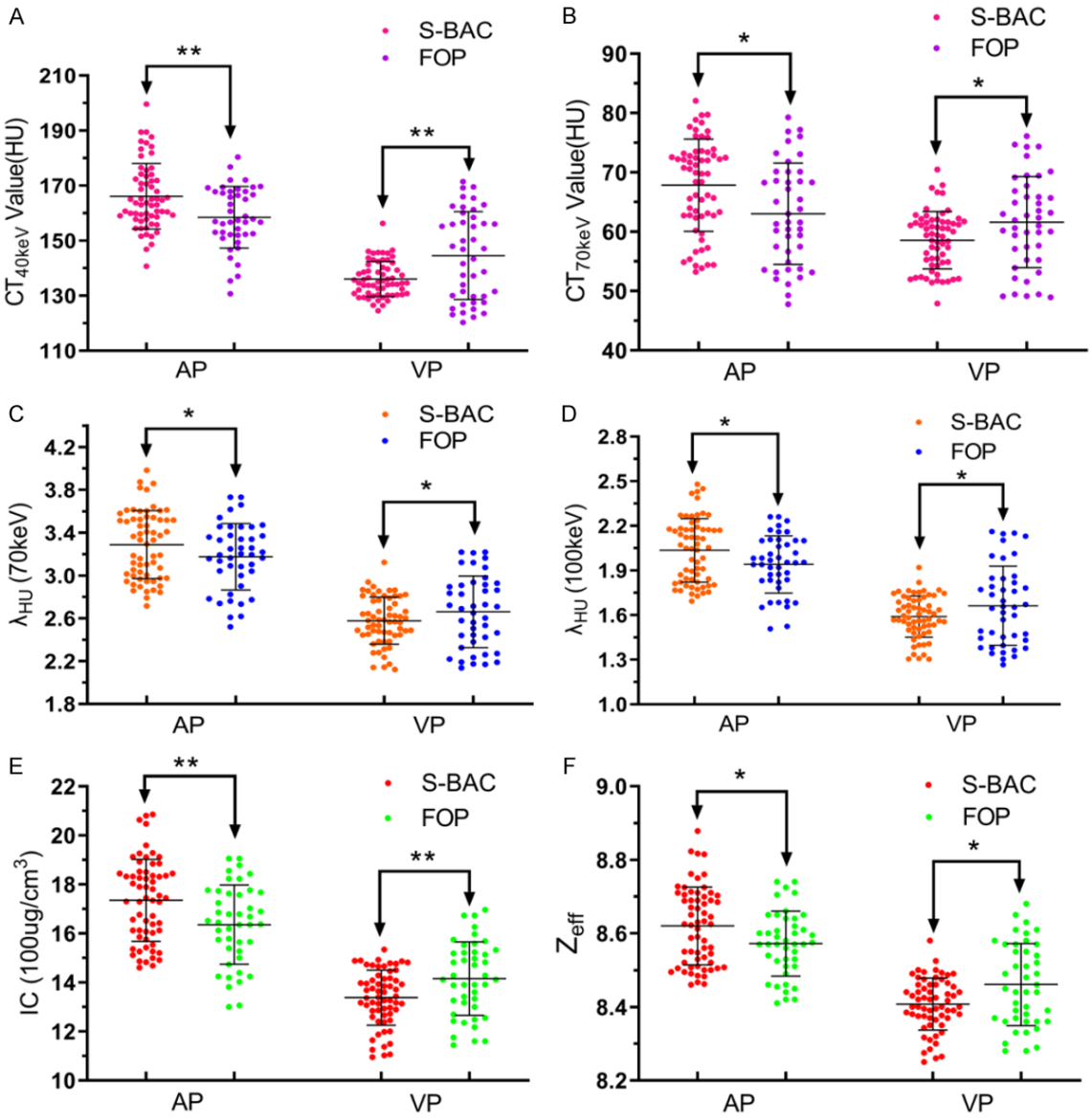

Figure 3. Scatter plots of the dual-energy spectral attenuation parameters for solitary bronchioloalveolar carcinoma (S-BAC) and focal organizing pneumonia (FOP). Long and short horizontal lines represent mean and error bars, respectively. AP, arterial phase; FOP, focal organizing pneumonia; VP, venous phase. *P < 0.05; **P < 0.01. (A, B) Scatter plots of (A) $CT_{40\ keV}$ value and (B) $CT_{70\ keV}$ value in AP and VP for S-BAC and FOP. (C, D) Scatter plots of (C) $\lambda_{70\ keV}$ and (D) $\lambda_{100\ keV}$ in AP and VP for S-BAC and FOP. (E, F) Scatter plots of (E) iodine concentration (IC) and (F) effective atomic number (Zeff) in AP and VP for S-BAC and FOP.

patients with FOP, its CT value (HU), IC and λ_{HU} are lower than those of patients with FOP. Our results are inconsistent with those reported by Hou et al. [19], who found that CT number (HU), NIC, and λ_{HU} were significantly higher in patients with inflammatory masses than in lung cancer patients during AP and VP. This may be due to the limited sample size, the lack of further subtype classification, and comparison between inflammatory masses and lung cancer. Moreover, in the results, only λ_{HU} was statistically significant in inflammatory masses and lung cancer patients. In our study, only two subtypes of S-BAC and FOP were analyzed, and our sample size was larger. In addition, our study found that the CT values of FOP and S-BAC at low keV (40 keV) were statistically different, while that at high keV (100 keV) were not. The difference is

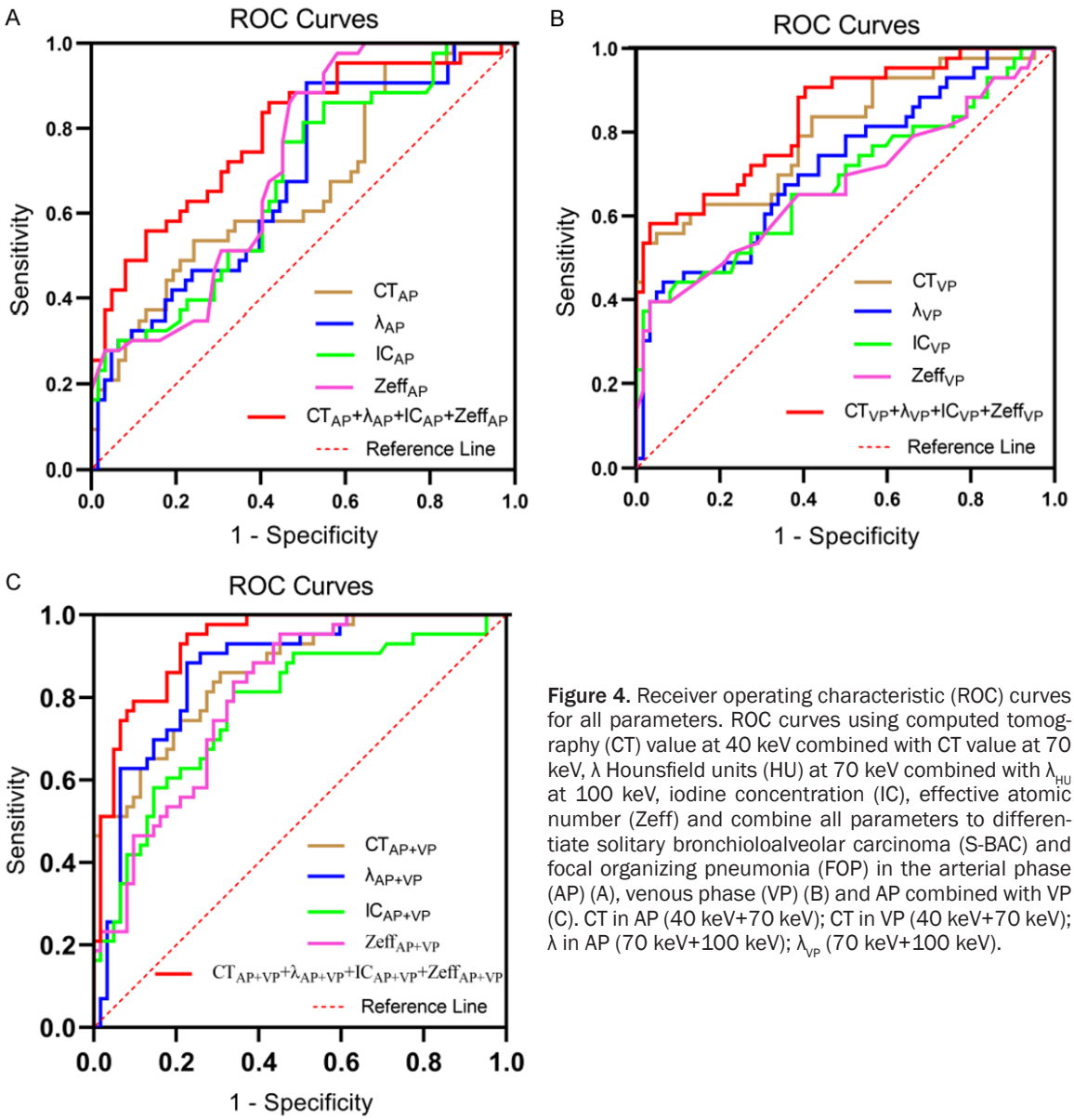

Figure 4. Receiver operating characteristic (ROC) curves for all parameters. ROC curves using computed tomography (CT) value at 40 keV combined with CT value at 70 keV, λ Hounsfield units (HU) at 70 keV combined with λ_{HU} at 100 keV, iodine concentration (IC), effective atomic number (Zeff) and combine all parameters to differentiate solitary bronchioloalveolar carcinoma (S-BAC) and focal organizing pneumonia (FOP) in the arterial phase (AP) (A), venous phase (VP) (B) and AP combined with VP (C). CT in AP (40 keV+70 keV); CT in VP (40 keV+70 keV); λ in AP (70 keV+100 keV); λ_{VP} (70 keV+100 keV).

because iodine decays more at lower energies; and the enhancement differences between the two groups were amplified when lower energy was used. This is consistent with the research results of Hou et al. [19].

ROC curve analysis revealed that the combination of all quantitative parameters in AP and VP demonstrated higher sensitivity and specificity (95.3% and 77.4%, respectively) in distinguishing S-BAC from FOP compared with AP and VP parameters alone. In addition, the slope of AP combined with that of VP also demonstrated high sensitivity and specificity (88.4% and 77.4%, respectively). Combining AP with VP parameters yielded the best sensitivity and specificity compared with quantitative parameters using AP or VP alone (**Table 3**; **Figure 4**). However, the thresholds evaluated in this study were based on a specific population, and the accuracy of these values need to be further confirmed in studies with larger sample sizes. These findings suggest that spectral CT is a promising approach to distinguish S-BAC from FOP and may facilitate clinical individualized treatment.

Our study had several limitations. First, the sample size was relatively small; however, it is a technical feasibility study with a statistical

Table 3. Performance of differential parameters in distinguishing S-BAC and FOP in ROC analysis

Parameter	AUC	YI	Threshold	Sensitivity (%)	Specificity (%)
AP					
CT_{AP}	0.662	0.293	0.475	53.5	75.8
λ_{AP}	0.674	0.391	0.318	90.7	48.4
IC	0.674	0.316	17.270	54.8	76.7
Zeff	0.714	0.416	8.621	53.2	88.4
$CT_{AP}+\lambda_{AP}$+IC+Zeff	0.787	0.441	0.293	86.0	61.9
VP					
CT_{VP}	0.802	0.519	0.673	53.5	98.4
λ_{VP}	0.722	0.377	0.545	44.2	93.5
IC	0.686	0.363	14.895	39.5	96.8
Zeff	0.680	0.363	8.505	39.5	96.8
$CT_{VP}+\lambda_{VP}$+IC+Zeff	0.839	0.549	0.643	58.1	96.8
AP+VP					
CT_{AP+VP}	0.864	0.554	0.263	86.0	69.4
λ_{AP+VP}	0.866	0.658	0.385	88.4	77.4
IC_{AP+VP}	0.776	0.475	0.379	81.4	66.1
$Zeff_{AP+VP}$	0.805	0.502	0.226	95.3	54.8
$CT_{AP+VP}+\lambda_{AP+VP}+IC_{AP+VP}+Zeff_{AP+VP}$	0.931	0.728	0.283	95.3	77.4

AP: Arterial phase, AUC: Area under cure, CT_{AP}: CT_{AP} (40 keV+70 keV), CT_{VP}: CT_{VP} (40 keV+70 keV), IC: Iodine concentration, VP: Venous phase, YI: Youden index, Zeff: Effective atomic number, λ_{AP}: λ_{AP} (70 keV+100 keV), λ_{VP}: λ_{VP} (70 keV+100 keV).

power over 0.8 at a significance level of 0.05. Second, the focus of this study was to distinguish S-BAC from FOP. In the future, more cases of lung cancer and inflammatory masses of different pathological types need to be investigated to draw broader conclusions. Third, to limit the dose of CT radiation, only a few patients simultaneously underwent non-contrast-enhanced chest CT scans by spectral imaging. There was an insufficient number of cases to compare the differences between spectral CT parameters before and after contrast-enhanced chest CT spectral imaging.

In conclusion, spectral CT using quantitative parameters improve the accuracy of distinguishing S-BAC from FOP.

Disclosure of conflict of interest

None.

Address correspondence to: Dr. Junlin Zhou, Department of Radiology, Lanzhou University Second Hospital, Cuiyingmen No. 82, Chengguan District, Lanzhou 730030, China. Tel: +86-0931-8942595; E-mail: ery_zhoujl@lzu.edu.cn

References

[1] Kohno N, Ikezoe J, Johkoh T, Takeuchi N, Tomiyama N, Kido S, Kondoh H, Arisawa J and Kozuka T. Focal organizing pneumonia: CT appearance. Radiology 1993; 189: 119-123.

[2] Yang PS, Lee KS, Han J, Kim EA, Kim TS and Choo IW. Focal organizing pneumonia: CT and pathologic findings. J Korean Med Sci 2001; 16: 573-578.

[3] Harris K, Puchalski J and Sterman D. Recent advances in bronchoscopic treatment of peripheral lung cancers. Chest 2017; 151: 674-685.

[4] Kilaru H, Jalna MV, Kilaru SC, Nandury EC and Khan M. Focal organizing pneumonia simulating lung malignancy: treated with prednisolone. Respirol Case Rep 2019; 7: e00469.

[5] Cordier JF. Organising pneumonia. Thorax 2000; 55: 318-328.

[6] McLoud TC, Epler GR, Colby TV, Gaensler EA and Carrington CB. Bronchiolitis obliterans. Radiology 1986; 159: 1-8.

[7] Kuhn C. Patterns of lung repair. A morphologist's view. Chest 1991; 99 Suppl: 11S-14S.

[8] Kim TS, Han J, Kim GY, Lee KS, Kim H and Kim J. Pulmonary inflammatory pseudotumor (inflammatory myofibroblastic tumor): CT features with pathologic correlation. J Comput Assist Tomogr 2005; 29: 633-639.

[9] Maldonado F, Daniels CE, Hoffman EA, Yi ES and Ryu JH. Focal organizing pneumonia on surgical lung biopsy: causes, clinicoradiologic features, and outcomes. Chest 2007; 132: 1579-1583.
[10] Lazor R, Vandevenne A, Pelletier A, Leclerc P, Court-Fortune I and Cordier JF. Cryptogenic organizing pneumonia. Characteristics of relapses in a series of 48 patients. The Groupe d'Etudes et de Recherche sur les Maladles "Orphelines" Pulmonaires (GERM"O"P). Am J Respir Crit Care Med 2000; 162: 571-577.
[11] Chen SW and Price J. Focal organizing pneumonia mimicking small peripheral lung adenocarcinoma on CT scans. Australas Radiol 1998; 42: 360-363.
[12] Watanabe K, Harada T, Yoshida M, Shirakusa T, Iwasaki A, Yoneda S and Kikuchi M. Organizing pneumonia presenting as a solitary nodular shadow on a chest radiograph. Respiration 2003; 70: 507-514.
[13] Ackerman LV, Elliott GV and Alanis M. Localized organizing pneumonia; its resemblance to carcinoma; a review of its clinical, roentgenographic and pathologic features. Am J Roentgenol Radium Ther Nucl Med 1954; 71: 988-996.
[14] Kim EY, Kim YS, Park I, Ahn HK, Cho EK, Jeong YM and Kim JH. Evaluation of sarcopenia in small-cell lung cancer patients by routine chest CT. Support Care Cancer 2016; 24: 4721-4726.
[15] Phillips M, Bauer TL, Cataneo RN, Lebauer C, Mundada M, Pass HI, Ramakrishna N, Rom WN and Vallieres E. Blinded validation of breath biomarkers of lung cancer, a potential ancillary to chest CT screening. PLoS One 2015; 10: e0142484.
[16] De Cecco CN, Darnell A, Rengo M, Muscogiuri G, Bellini D, Ayuso C and Laghi A. Dual-energy CT: oncologic applications. AJR Am J Roentgenol 2012; 199 Suppl: S98-S105.
[17] Fornaro J, Leschka S, Hibbeln D, Butler A, Anderson N, Pache G, Scheffel H, Wildermuth S, Alkadhi H and Stolzmann P. Dual- and multi-energy CT: approach to functional imaging. Insights Imaging 2011; 2: 149-159.
[18] Aoki M, Takai Y, Narita Y, Hirose K, Sato M, Akimoto H, Kawaguchi H, Hatayama Y, Miura H and Ono S. Correlation between tumor size and blood volume in lung tumors: a prospective study on dual-energy gemstone spectral CT imaging. J Radiat Res 2014; 55: 917-923.
[19] Hou WS, Wu HW, Yin Y, Cheng JJ, Zhang Q and Xu JR. Differentiation of lung cancers from inflammatory masses with dual-energy spectral CT imaging. Acad Radiol 2015; 22: 337-344.
[20] Chae EJ, Song JW, Krauss B, Song KS, Lee CW, Lee HJ and Seo JB. Dual-energy computed tomography characterization of solitary pulmonary nodules. J Thorac Imaging 2010; 25: 301-310.
[21] Swensen SJ, Viggiano RW, Midthun DE, Muller NL, Sherrick A, Yamashita K, Naidich DP, Patz EF, Hartman TE, Muhm JR and Weaver AL. Lung nodule enhancement at CT: multicenter study. Radiology 2000; 214: 73-80.
[22] Zhang M and Kono M. Solitary pulmonary nodules: evaluation of blood flow patterns with dynamic CT. Radiology 1997; 205: 471-478.
[23] Austin JH, Garg K, Aberle D, Yankelevitz D, Kuriyama K, Lee HJ, Brambilla E and Travis WD. Radiologic implications of the 2011 classification of adenocarcinoma of the lung. Radiology 2013; 266: 62-71.
[24] Zhao F, Yan SX, Wang GF, Wang J, Lu PX, Chen B, Yuan J, Zhang SZ and Wang YX. CT features of focal organizing pneumonia: an analysis of consecutive histopathologically confirmed 45 cases. Eur J Radiol 2014; 83: 73-78.
[25] Yazdani S, Miki Y, Tamaki K, Ono K, Iwabuchi E, Abe K, Suzuki T, Sato Y, Kondo T and Sasano H. Proliferation and maturation of intratumoral blood vessels in non-small cell lung cancer. Hum Pathol 2013; 44: 1586-1596.